
Yuta Seo¹

Satoru Masubuchi¹, Kenji Watanabe², Takashi Taniguchi¹,
and Tomoki Machida^{1, 3}

¹Institute of Industrial Science, University of Tokyo, Tokyo 153-8505, Japan

²National Institute for Materials Science, Tsukuba 305-0044, Japan

³CREST-JST, Japan

yu-seo@iis.u-tokyo.ac.jp

Subband-resolved resonant tunneling in trilayer graphene/ h-BN/graphene heterostructures

Trilayer graphene (TLG) has a unique electronic band structure consisting of monolayer-graphene-like (MLG-like) and bilayer-graphene-like (BLG-like) subbands, and shows interesting physical phenomena such as Landau level crossing and mixing [1]. Here we study tunneling transport in TLG/hexagonal boron nitride (h-BN)/MLG van der Waals (vdW) heterostructures in which a thin h-BN layer works as a tunnel barrier. We observe resonant tunneling between each TLG's subband and MLG.

Figures 1a,b show the schematic diagram and optical micrograph of our TLG/h-BN/MLG tunnel device. Our device is fabricated by stacking mechanically-exfoliated graphene and h-BN flakes with the stamping method, and the crystallographic orientation of TLG and MLG are aligned to 1 degree during the stacking procedure (Figs. 1b-d). In this device, we carry out tunneling transport measurements at $T = 30$ mK while controlling the Fermi levels in TLG and MLG by applying interlayer bias V_b and backgate voltage V_{bg} (Fig. 2a). Figure 2b shows the dependence of measured current density J as a function of interlayer bias V_b at three different values of backgate voltage ($V_{bg} = -40, 0, 40$ V). In $J(V_b)$ at $V_{bg} = -40, 40$ V, we observe peak structures indicated by black arrows, followed by regions of negative differential conductance (NDC). To study the tunneling transport in detail, we measure differential conductance dI/dV and observe complicated peak structures. Figure 2c shows the color plot of dI/dV as a function of V_b and V_{bg} , and the regions of NDC are shown as green areas. To understand these peak structures, we calculate the band alignment of TLG and MLG along the energy E direction and the momentum k_y direction at various V_b and V_{bg} as shown in Figs. 3(i)-(iii), based on the tight-binding approximation and the three-plate capacitor model. Figure 3d shows the positions of resonant conditions from the theoretical calculations, where either the Fermi level of TLG or MLG locates on intersections between MLG and each of TLG's subbands as shown in Figs. 3a-c, and electrons can tunnel the energy barrier resonantly with energy and momentum conserved. Blue, red, and green lines in Fig. 3d correspond to the three types of resonant conditions (I) between MLG and low-energy BLG-like band of TLG (Fig. 3a), (II) between MLG and MLG-like band of TLG (Fig. 3b), and (III) between MLG and high-energy BLG-like band of TLG (Fig. 3c), respectively. Figures 3(i)-(iii) show the band alignments at positions (i)-(iii) in Fig. 3d. In the case of Figs. 3(i),(iii), the overlap of MLG band and TLG band is small, so we observe small resonant peaks. In the case of Fig. 3(ii), the overlap of MLG band and TLG's MLG-like band is large, so we observe large resonant peaks followed by NDC. Comparing measured data with theoretical calculations, we confirm that the electronic band structure of TLG consists of MLG-like and BLG-like subbands.

In a magnetic field up to $B = 9$ T, we observe complicated peak structures in dI/dV (Fig. 4a). We calculate the positions where the Fermi level of MLG locates on the MLG's Landau levels (LLs) (Fig. 4b①) and TLG's LLs (Fig. 4b④) and the Fermi level of TLG locates on TLG's LLs (Fig. 4b③) and MLG's LLs (Fig. 4b②). This calculation explains the measured peak structures well and we attribute the peak structures to electron tunneling between TLG's LLs and MLG's LLs as shown in the inset of Fig. 4a.

References

[1] Y. Asakawa, S. Masubuchi, N. Inoue, S. Morikawa, K. Watanabe, T. Taniguchi, and T. Machida. Phys. Rev. Lett. **119**,186802 (2017).

Figures

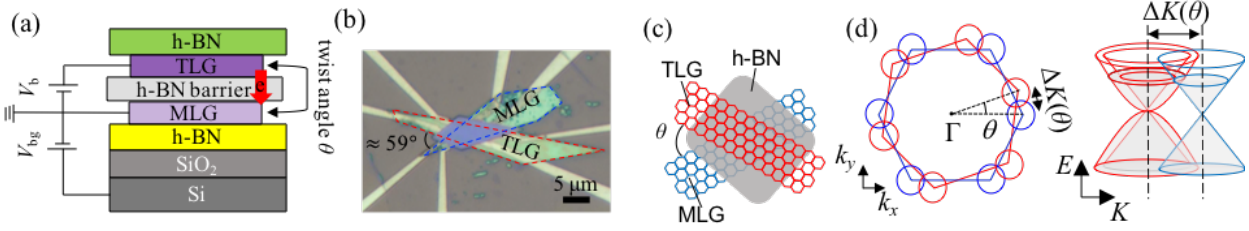


Figure 1 (a) Schematic diagram of the TLG/h-BN/MLG tunnel device. (b) Optical micrograph of the device. (c,d) Schematics of twist angle θ (c) in the real space and (d) in the momentum space.

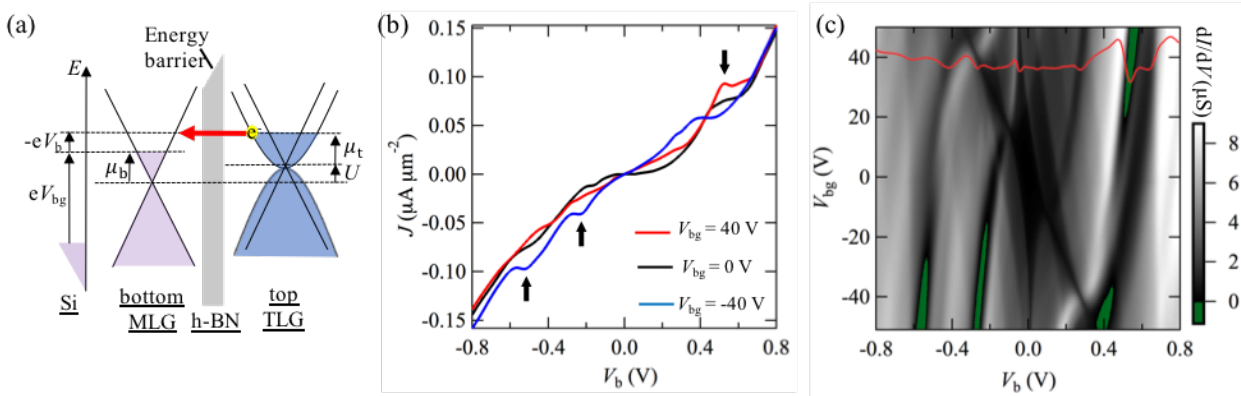


Figure 2 (a) Simplified energy diagram of the tunnel device. (b) Measured current density-voltage curves at different V_{bg} . (c) Measured dI/dV color plot as a function of V_b and V_{bg} . Red curve shows dI/dV at $V_{bg} = 40$ V.

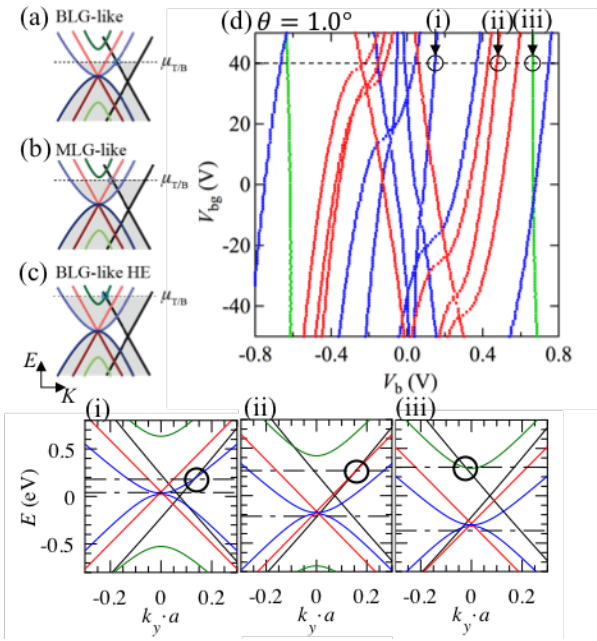


Figure 3 Theoretical calculation of resonant conditions. (a-c) Schematics of resonant conditions. (d) Positions of resonant conditions as a function of V_b and V_{bg} . (i-iii) Band alignments at each position (i)-(iii) in (d).

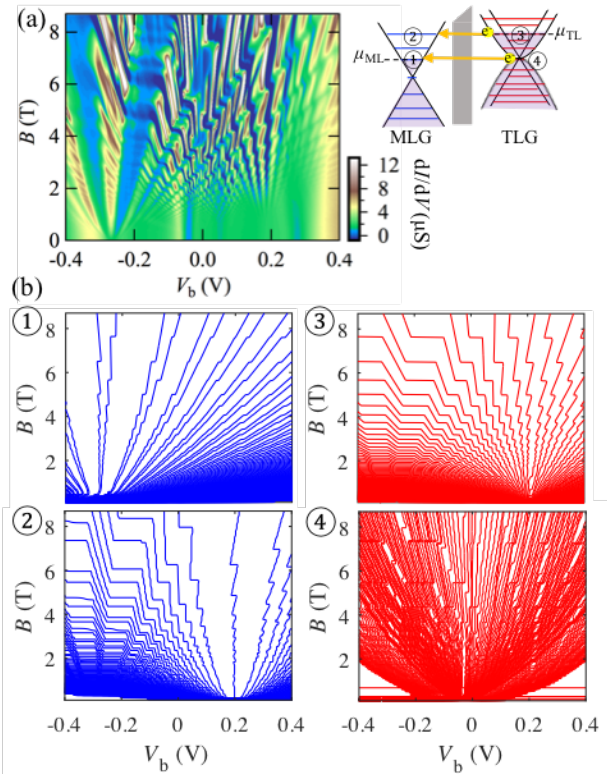


Figure 4 (a) Measured dI/dV plot as a function of V_b and B at $V_{bg} = 40$ V. (b) Calculated contour plots of LLs indicated by ①-④ in the inset of (a).